Biomaterials Science

ROYAL SOCIETY OF CHEMISTRY

PAPER

View Article Online
View Journal | View Issue

Cite this: *Biomater. Sci.*, 2023, **11**, 3197

Cellular energy supply for promoting vascular remodeling of small-diameter vascular grafts: a preliminary study of a new strategy for vascular graft development†

Hengxian Su, ‡[a] Wenchao Liu,‡[a] Xifeng Li,‡[a] Guangxu Li,[a] Shenquan Guo,[a] Chang Liu,[e] Tao Yang,[a] Chubin Ou,[a] Jiahui Liu,[a] Yuanzhi Li,[a] Chengcong Wei,[a] Qing Huang,*[d] Tao Xu*[b,c] and Chuanzhi Duan *[a]

Rapid endothelialization is extremely essential for the success of small-diameter tissue-engineered vascular graft (TEVG) (<6 mm) transplantation. However, severe inflammation *in situ* often causes cellular energy decline of endothelial cells. The cellular energy supply involved in vascular graft therapy remains unclear, and whether promoting energy supply would be helpful in the regeneration of vascular grafts needs to be established. In our work, we generated an AMPK activator (5-aminoimidazole-4-carboxamide ribonucleotide, AICAR) immobilized vascular graft. AICAR-modified vascular grafts were successfully generated by the co-electrospinning technique. *In vitro* results indicated that AICAR could upregulate energy supply in endothelial cells and reprogram macrophages (MΦ) to assume an anti-inflammatory phenotype. Furthermore, endothelial cells (ECs) co-cultured with AICAR achieved higher survival rates, better migration, and angiogenic capacity than the controls. Concurrently, a rabbit carotid artery transplantation model was used to investigate AICAR-modified vascular grafts at different time points. The results showed that AICAR-modified vascular grafts had higher patency rates (92.9% and 85.7% at 6 and 12 weeks, respectively) than those of the untreated group (11.1% and 0%). In conclusion, AICAR strengthened the cellular energy state and attenuated the adverse effects of inflammation. AICAR-modified vascular grafts achieved better vascular remodeling. This study provides a new perspective on promoting the regeneration of small-diameter vascular grafts.

Received 22nd August 2022,
Accepted 22nd February 2023

DOI: 10.1039/d2bm01338j

rsc.li/biomaterials-science

1. Introduction

Cardiovascular disease (CVD) is reported as the leading cause of death worldwide. Coronary-artery bypass grafting using autologous vessels is considered as the current gold standard for severe cases of CVD.[1–3] However, autologous vessels, such as the radial artery and saphenous vein, are not always suitable for grafting due to additional pain caused by transplantation and severe shortages of donor tissue.[4–6] Thus, tissue-engineered vascular grafts (TEVGs) with good regenerative potential are very promising in coronary-artery bypass grafting.

In recent decades, many efforts have been made to improve surface modification techniques, which are viewed as effective and simple ways to functionalize the grafts, including physical immobilization, surface adsorption, plasma treatment and chemical immobilization.[8] These methods mostly focus on grafting some biological biomacromolecules onto the TEVGs, like growth factors, DNA or drugs, thereby enhancing cell recruitment, adhesion, growth and proliferation, as well as angiogenesis and anticoagulation. Despite some improve-

[a]*Neurosurgery Center, Department of Cerebrovascular Surgery, The National Key Clinical Specialty, The Engineering Technology Research Center of Education Ministry of China on Diagnosis and Treatment of Cerebrovascular Disease, Guangdong Provincial Key Laboratory on Brain Function Repair and Regeneration, The Neurosurgery Institute of Guangdong Province, Zhujiang Hospital, Southern Medical University, Guangzhou 510280, China. E-mail: doctor_duanzj@163.com*
[b]*Biomanufacturing and Rapid Forming Technology Key Laboratory of Beijing, Department of Mechanical Engineering and Key Laboratory for Advanced Materials Processing Technology, Ministry of Education, Department of Mechanical Engineering, Tsinghua University, Beijing 100084, People's Republic of China. E-mail: taoxu@mail.tsinghua.edu.cn*
[c]*East China Institute of Digital Medical Engineering, Shangrao, 334000, China*
[d]*Department of Neurosurgery, Beijing Luhe Hospital, Capital Medical University, Beijing 101149, China. E-mail: huangqing@ccmu.edu.cn*
[e]*Department of Orthopedic Surgery, The Lingnan Hospital of Sun Yat-Sen University, Guangzhou, 510630, China*

†Electronic supplementary information (ESI) available. See DOI: https://doi.org/10.1039/d2bm01338j

‡These authors contributed equally to this work.

ments having been made in TEVG fabrication, these processes cannot fully meet the need for clinical application because of unfavorable endothelial cell formation and vascular remodeling. The surface modification techniques still need to be optimized. Finding effective modification methods and achieving effective endothelialization remain the primary challenge for small-diameter TEVG applications.

Given past research, the early stage formation of ECs onto the lumen of TEVGs is essential for successful grafting.[7–10] Unfavorable factors such as mechanical injury and inflammatory responses damage ECs and expose extracellular matrix (ECM) proteins such as collagen, which can then trigger thrombosis. Therefore, healthy ECs play important roles in maintaining vascular grafts' patency.[11–13] However, the transplantation process itself, as well as immune rejection of TEVGs, damages EC blood vessels and provokes sustained inflammatory responses, leading to subsequent intimal hyperplasia and inadequate endothelialization of artificial grafts.[14–17] To successfully initiate endothelium remodeling, the associated inflammation response in TEVGs must be reduced.[18–21]

Notably, promoting inflammation resolution is an important factor influencing tissue regeneration.[22] In particular, among all the immune cells, macrophages (MΦ) polarized into the M2 phenotype can alleviate the inflammatory response and participate in the tissue remodeling process. In contrast, the M1 phenotype can stimulate host immune reactions and express pro-inflammatory cytokines.[20,23,24] Therefore, stimulating MΦ polarization toward an M2 phenotype and attenuating the M1 phenotype offers a promising solution to enhance vascular graft remodeling.

AMP-activated protein kinase (AMPK), ubiquitously expressed in all eukaryotic cells, is a central metabolic regulator with established anti-inflammatory actions. AMPK can be activated in the low energy state in response to the increase of AMP : ATP and ADP : ATP ratios.[25] The importance of metabolism in regulating immunity and inflammation is now widely recognized.[26,27] The anti-inflammatory potential of AMPK is extremely attractive as it can be used to protect cells or tissues from inflammatory damage and to promote survival. AICA riboside (AICAR; 5-amino-4-imidazole carboxamide riboside), an activator of AMPK, was reported to have anti-inflammatory effects in myocytes, adipocytes, and macrophages grown in culture, and on muscle and adipose tissue of lipopolysaccharide (LPS)-treated rats.[28] Moreover, AMPK activators have been found to ameliorate endothelial dysfunction associated with inflammation and maintain energy supply.[29–31] Taken together, the data demonstrate that AMPK activators can alleviate inflammation and maintain energy supply in cells, which is an extremely promising strategy to support prolonged cell health in grafts.

Herein, we successfully prepared electrospun TEVGs by blending PLLA and gelatin to synthesize a graft integrated with an AMPK activator (AICAR). The chemical and physical properties of the fabricated TEVGs were evaluated. The effects of the AICAR *in vitro* on cellular energy regulation, anti-inflammatory activity and macrophage polarization were assessed. TEVGs were also implanted into New Zealand white rabbits to evaluate the patency rate, histological changes and endothelialization. To our knowledge, we are the first to report that upregulation of cellular energy supply along with macrophage polarization toward the M2 phenotype, induced by an AMPK activator (AICAR), contributes to vascular remodeling of TEVGs.

2. Materials and methods

2.1 Materials

AICAR (A8184) and compound C (B3252) were purchased from APExBIO (Houston, TX, USA). LPS (from *Escherichia coli*, 055: B5) was obtained from Sigma-Aldrich (St Louis, MO, USA). HUVECs were purchased from ScienCell (San Diego, CA, USA). Interleukin (IL)-6/IL-8 ELISA kits were purchased from MLbio (Shanghai, China). Codex EnerCount™ Cell Growth Assay Kits (CB-80551-100) were purchased from Codex Biosolutions, Inc. (Gaithersburg, MD, USA). The JC-1 dye kit and Live & Dead Viability/Cytotoxicity Assay Kit were purchased from KeyGEN BioTECH (Nanjing, China). The anti-α-SMA antibody was purchased from Sigma-Aldrich. The anti-CD31 antibody was purchased from NOVUS Company (Littleton, MA, USA).

2.2 Preparation of the tissue engineered blood vascular grafts

AICAR was dissolved in dimethyl sulfoxide to form a 400 mM concentration composite solution. The biodegradable polymers PLLA and gelatin, with a defined weight ratio (3 : 1), were mixed to form 15% (wt/v) mixture solution in 1,1,1,3,3,3-hexafluoro-2-propanol. The electrospinning composition with AICAR (final concentration: 8 mM) was generated by blending the polymer solution with AICAR; similarly, the electrospinning composition without AICAR was obtained with an equal volume of dimethyl sulfoxide instead of AICAR. The process of how AICAR concentration is used within the vascular graft was determined and can be seen in the ESI (Fig. S1†). TEVGs with or without AICAR were fabricated using a self-assembled electrospinning setup. The electrospinning composition was delivered at a flow rate of 4 mL h^{-1} using an adjustable syringe pump which was connected to a 23-gauge stainless-steel needle. The collector was a stainless-steel rod (diameter = 1 mm; length = 10 cm) which was connected to a rotating motor (speed = 100 rpm). A needle-to-collector distance of 14 cm and a positive voltage of 16 kV were applied during electrospinning. Electrospinning was continued until the wall thickness of the graft reached approximately 200 μm. Then, grafts were removed from the collector rod and placed into a 37 °C desiccator overnight to remove any residual solvent. The grafts were cut to a length of 8 mm each for vascular graft implantation.

2.3 Characterization of vascular grafts

2.3.1 Tensile strength. Tensile strength was evaluated by using an Instron machine (MTS E43.104, Shenzhen, China).

Tubular vascular grafts (n = 5 for all groups) were cut to a length of 1 cm and were wetted with phosphate-buffered saline (PBS) before being placed onto the Instron machine. A strain rate of 100 mm s^{-1} was applied and the grafts were stretched until a fracture occurred. The final tensile strength was recorded and compared with previously reported data of native arteries.

2.3.2 FTIR. Electrospun tubular grafts were carefully cut into 3 mm × 3 mm rectangular segments and analyzed by FTIR (FTIR-650, Tianjin, China). The fabricated samples were measured in transmittance mode in the range of 800–2000 cm^{-1}. The position of the peaks in AICAR and the AICAR-modified vascular grafts was analyzed by comparing with previously reported values.

2.3.3 AICAR-release test. AICAR-modified tubular grafts that were 2 cm in length and 13 mg in weight were placed in 2 mL of PBS and kept at 37 °C. At different time points (1, 4, 6, 9, 12, 15, and 18 days), 100 μL of the supernatant was harvested and the concentration of AICAR was detected by using a NanoDrop spectrophotometer (Waltham, MA, USA). In brief, AICAR was dissolved in PBS to form standard dilutions with concentrations from 0.0195 mM to 5 mM. The absorbance values of standard dilutions were determined and applied to create a standard curve. According to the standard curve, the AICAR concentration of each sample was determined.

2.3.4 Degradation analysis. The value of the degradation rate was defined as a percentage weight loss that is expressed in dry vascular grafts. The amount of AICAR loaded was quite small, thus the degradation rate of non-AICAR grafts could be regarded as that of all fabricated grafts. Samples without AICAR (approximately 2 cm in length and 13 mg in weight) were divided into six groups (each group n = 3) and incubated with 2 mL of PBS for various durations (1, 3, 6, 9, 12, and 15 weeks). PBS was renewed every week. Each graft was weighed at the beginning of the test. At the end of each time point, the corresponding samples were dried using a vacuum machine and then weighed. W_1 and W_2 were defined as the weight of the specimens before and after the degradation. The degradation rate was calculated by using the following formula:

$$\text{Degradation rate } (\%) = (W_1 - W_2)/W_1 \times 100\%$$

2.3.5 SEM. The morphology of the fabricated grafts was examined using SEM. The electrospun grafts were cut into pieces (5 × 5 mm) and kept in a vacuum machine overnight to remove residual water. Dried samples were placed on a holder and sputter coated with gold before observation using SEM. An extra high tension of 5 kV was applied to the SEM examination.

2.3.6 Static contact angle. The wettability of the TEVG materials was examined using a contact angle meter Kino SL250 (Boston, MA, USA) by the sessile drop method. 4 μl of deionized water was dropped onto the samples with a surface area of 2 × 2 cm^2. The average contact angle of three test points for each sample was taken as the measurement result.

2.4 *In vitro* study of AICAR

2.4.1 Cell culture. Commercially available HUVECs and RAW264.7 macrophages were obtained from ScienCell (San Diego, CA, USA). Cells were cultured in Minimum Essential Medium (MEM, Gibco) supplemented with 10% fetal bovine serum (FBS, Gibco) at 37 °C under a humidified atmosphere with 5% CO_2. First, the effectiveness of several diverse concentrations (0.1, 0.2, 0.5, 1 and 2 mM) of AICAR on the viabilities of HUVECs was evaluated. The appropriate concentration was confirmed to be 1 mM (Fig. S2, ESI†), which was used in the next experiments. The HUVECs and RAW264.7 macrophages were treated with 10 μg mL^{-1} LPS for 24 h to form cell inflammation models prior to the subsequent *in vitro* cell experiments. The cells utilized in this experiment were between passages three and eight.

2.4.2 Cellular energy supply detection and the anti-inflammatory properties of AICAR. The concentration of cellular ATP was determined using an EnerCount Cell Growth Assay Kit. Mitochondrial Membrane Potential (MMP) was detected by laser confocal scanning microscopy and flow cytometry using a JC-1 probe. IL-6 and IL-8 ELISA kits and quantitative real-time polymerase chain reaction (qRT-PCR) were used to evaluate the anti-inflammatory properties of AICAR. Briefly, HUVECs were incubated in 6-well plates with 24 h of LPS-induced treatment. Then, equal amounts of culture medium (control group), 1 mM AICAR (AICAR group), and 1 mM AICAR + 10 μM compound C (inhibitor group) were added to the corresponding groups for 24 h incubation. After 24 h treatment, the culture supernatants were harvested to measure the concentrations of IL-6 and IL-8 using ELISA kits. The HUVECs of each group were stained using a JC-1 dye kit to measure MMP, or trypsinized, resuspended, and subjected to ATP detection and qRT-PCR. For qRT-PCR, the primer sequences are listed in Table S1 (ESI†); fold changes in gene expression were determined relative to the blank control after normalization to 18S ribosomal RNA expression using the $2^{-\Delta\Delta Ct}$ method. All the procedures mentioned above were performed according to the manufacturer's protocols.

2.4.3 Western blotting. The HUVECs of each group were lysed in cell lysis buffer for western blotting with 1 mM phenylmethanesulfonyl fluoride (PMSF, Beyotime, Shanghai, China). Protein concentrations were measured using the BCA assay. 40 μg of protein were separated on 12% SDS-PAGE gels for 1.5 h at 100 V and then transferred to a 0.45 μm nitrocellulose membrane. The membrane was blocked with 5% non-fat dry milk at room temperature for 1 h. The membrane was incubated with a primary antibody against AMPK or p-AMPK (Thr 172, 1 : 1000; Affinity Biosciences, OH, USA) for 24 h at 4 °C. The secondary antibody was goat anti-rabbit IgG (H + L) (1 : 10 000, Affinity Biosciences, OH, USA). The blots were visualized using the Affinity ECL kit and quantification of protein was performed using ImageJ software (National Institutes of Health, USA).

2.4.4 *In vitro* analysis of macrophage polarization. To study the effects of AICAR on macrophage polarization, the

phenotypes of stimulated MΦ in each group were determined by immunofluorescence and qRT-PCR analyses. Briefly, an appropriately shaped electrospun membrane with or without AICAR, made using the same procedure as that for the preparation of the vascular grafts, was placed on the bottom of a 48-well plate. RAW264.7 MΦ were seeded onto the membranes at a density of 10×10^4 cells per well. After 24 h of incubation, for immunofluorescence analysis, MΦ were incubated using the primary antibodies rat-anti-CD163 (1 : 100, Biolegend, CA, USA) and rabbit-anti-iNOS (1 : 100; Affinity Biosciences, OH, USA) overnight at 4 °C and stained with the secondary antibodies Alexa Fluor 488 goat anti-rat IgG (1 : 100, Bioss, Beijing, China) and Alexa Fluor 594 goat anti-mouse IgG (1 : 100, Bioss, Beijing, China) for 45 min at 24 °C. Next, the cell nuclei were stained with DAPI. Finally, MΦ were imaged using laser confocal scanning microscopy (LCSM, Zeiss LSM880, Jena, Germany). Quantification of the iNOS-M1 or CD163-M2 phenotype MΦ was performed using ImageJ software. For qRT-PCR, the primer sequences are listed in Table S2 (ESI†); quantitative analysis of gene expression was performed relative to the blank control after normalization to GAPDH ribosomal RNA expression using the $2^{-\Delta\Delta Ct}$ method. All the procedures mentioned above were performed according to the manufacturer's protocols.

2.4.5 Cell viability. A CCK-8 kit (Dojindo, Kyushu, Japan) was used to evaluate cell viability. Briefly, HUVECs (6×10^4 cells per well) were seeded onto 24-well culture plates in MEM with 10% FBS and treated with 10 μg mL^{-1} LPS for 24 h. The cells were divided into control group, AICAR group, and inhibitor group similar to those described above. After additional 24 h of incubation, the culture medium was removed and 50 μL of CCK-8 reagent were transferred into each well for 2 h of incubation. The absorbance of the supernatants at 450 nm was detected using a microplate reader (BioTek Instruments, Winooski, VT, USA). The rest of the cells were stained using a Live & Dead Viability Assay Kit to confirm the effects of AICAR on the viability of HUVECs. The images were obtained using a fluorescence microscope (Mshot, Guangzhou, China). To further observe the performance of HUVECs on the AICAR-modified membrane, SEM was used to visualize the adhesion of HUVECs on the membrane. All tests were repeated three times.

2.4.6 Cell wound scratch test. HUVECs were incubated to confluence in 6-well plates. After 24 h of LPS-induced treatment, a disposable 200 μL pipette was used to create a straight-line scratch on the culture plates. The cell debris was removed gently with PBS. The MEM culture medium with 10% FBS was replaced with serum-free MEM. The cells were incubated for another 24 h. The healing areas were photographed and calculated at the beginning and end of the examination (S_1 and S_2, respectively, referred to as the scratch areas before and after the test). The degree of healing, as an indicator of migration ability, was calculated using ImageJ software using the formula below. The test was repeated three times.

$$\text{Scratch healing } (\%) = (W_1 - W_2)/W_1 \times 100\%$$

2.4.7 Tube formation assay. To investigate the effect of AICAR on stimulating angiogenesis, a tube formation assay was carried out. Briefly, appropriately shaped electrospun membranes with or without AICAR were placed on the bottom of 48-well plates. After thawing on ice at 4 °C overnight, 100 μl of Matrigel (BD, Franklin Lake, NJ, USA) was added to each well of 48-well plates covering the electrospun membranes and allowed to solidify at 37 °C for 60 min in an incubator. HUVECs (5×10^4) pretreated with 24 h of LPS were seeded in each Matrigel-coated well and cultured at 37 °C under 5% CO_2 for 12 h. The tubular structures were observed through an optical microscope. The number of meshes, master segments and master junctions and the total master segment length were detected using an angiogenesis analyzer that is developed for ImageJ software.[32]

2.5 *In vivo* implantation and evaluation

2.5.1 Animals. All animal procedures were performed in accordance with the Guidelines for Care and Use of Laboratory Animals of the Southern Medical University (Guangzhou, Guangdong, China) and approved by the Animal Ethics Committee of the Southern Medical University. Adult male New Zealand white rabbits (2.0–2.2 kg) were purchased from the Guangdong Medical Laboratory Animal Center (Foshan, Guangdong, China). The rabbits were divided into AICAR group and control group, housed, and allowed free access to water and food. They were fasted for 12 h before surgery.

2.5.2 Surgical procedures and patency measurements. The rabbits utilized were first subjected to systemic half-heparinization (100 U kg^{-1}), and then anesthetized by slow auricular intravenous injection of 3% pentobarbital sodium (0.7 mL kg^{-1}) and placed in the supine position. The right common carotid artery (CCA) was exposed by making a midline ventral incision. Then, the right CCA was blocked with two vascular clamps and a fabricated vascular graft (8 mm in length) was sutured end-to-end to the right CCA with 11-0 sutures. The vascular clamps were reopened and the anastomosis was compressed using hemostatic gauze for several seconds until no active bleeding occurred. The incision was then sutured layer by layer. After surgery, aspirin (10 mg kg^{-1}) was administered orally daily for 1 week. At 6 and 12 weeks, the patency of grafts was measured using color Doppler ultrasound (8.5 MHz). At 12 weeks, digital subtraction angiography (DSA) was performed to visualize the patency of the implanted vascular grafts.

2.5.3 Tissue staining and endothelialization assessment. At each observation time period after implantation, the rabbits were euthanized and grafts were explanted and cleaned with PBS to remove any remaining blood. The implanted grafts were fixed in 4% formalin or 2.5% glutaraldehyde. Then, hematoxylin and eosin (H&E) staining, Masson's trichrome staining, and immunofluorescence staining for the endothelial marker CD31 and vascular smooth muscle cell (VSMC) marker α-SMA were performed to investigate the changes in histology and cytology. H&E and Masson's trichrome staining were performed using cross-cut specimens. Endothelialization of the inner surface was observed through SEM, and the immuno-

fluorescence images of $CD31^+$ areas (green or red) were used to visualize the presence of ECs.

To quantify the MΦ phenotypes present in the remodeling grafts, the vascular grafts were explanted at 6 and 12 weeks, and then frozen sections were prepared. Immunofluorescence analysis was performed with anti-CD163 antibodies (1 : 200; Novus) and anti-iNOS antibodies (1 : 500; Novus). Fluorescence quantitative analysis was performed after photographing.

2.6 Statistical analysis

The data were presented as mean ± standard deviation and compared by one-way ANOVA tests. Fisher's exact test was performed to evaluate significant differences between pairs in patency rate. A p-value of less than 0.05 was considered statistically significant.

3. Results

3.1 Morphology of the fabricated tubular grafts

The AICAR-modified small-diameter TEVGs were successfully generated by blending the bioabsorbable materials PLLA and gelatin. The fabricated grafts, with 1 mm inner diameter and 8.0 mm length, are shown in Fig. 1A and B. All of the grafts were electrospun using a self-assembled device (Fig. 1C). The microstructure and topography of the inner surface are shown in Fig. 1D and E. The average fiber diameter of the electrospun samples with or without AICAR was 0.812 ± 0.084 μm and 0.750 ± 0.102 μm, respectively, and showed no significant difference (Fig. 1F). The above results indicated that the addition of AICAR did not affect the microstructure of the tubular grafts.

3.2 Mechanical properties

An ideal synthetic graft for clinical use must meet the requirements of withstanding mechanical stress and mimicking the native blood vessels. In this context, the tensile strength of vascular grafts with and without AICAR was found to be 12.78 ± 0.44 MPa and 13.96 ± 1.32 MPa, respectively, and showed no significant difference (Fig. 1G). The data indicated that the tensile strength was not affected by the addition of AICAR. According to a previous study, the tensile strength of the human saphenous vein was 13.22 ± 5.73 MPa,[33] which was similar to that of our fabricated vascular grafts. Thus, the vascular grafts possessed an appropriate mechanical strength to be implanted into live animal models.

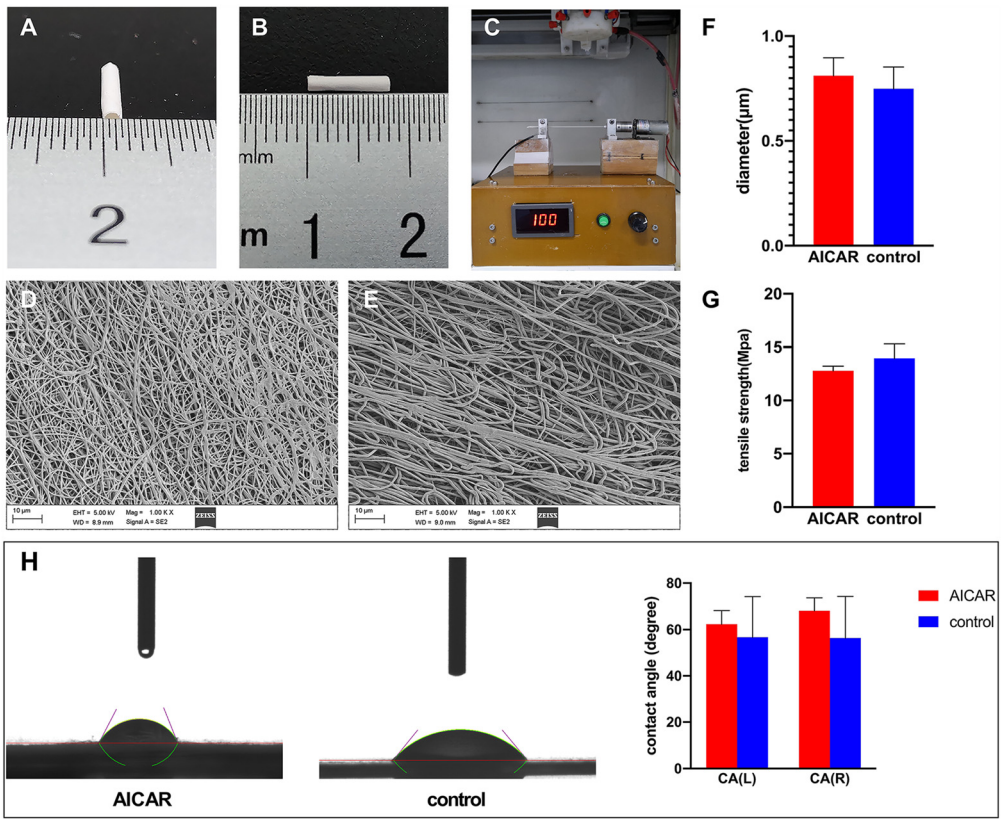

Fig. 1 Characterization of AICAR-modified and untreated vascular grafts. (A and B) Appearance of the fabricated grafts with 1 mm inner diameter and 8.0 mm length. (C) The self-assembled device was used as a nano-fiber collector to make vascular grafts. (D and E) The microstructure and topography of the inner surface of the AICAR-modified (D) and untreated (E) vascular grafts were observed by SEM. (F) The analysis of the average fiber diameter of the electrospun samples with or without AICAR (n = 18). (G) The comparison of tensile strength of vascular grafts with and without AICAR vascular grafts (n = 5). (H) Contact angle measurement of the samples (n = 3).

3.3 Contact angle analysis

The wetting property of vascular grafts was examined using a static contact angle test (Fig. 1H). The shape of the water droplets on the two types of materials was similar. The mean contact angles of the AICAR group and control group were 65.18° and 56.53°, respectively, showing no statistical difference. The contact angles of the two types of materials were less than 90°, indicating that both AICAR group and control group grafts had good hydrophilicity, which may be beneficial for EC adhesion.

3.4 Detection of AICAR, *in vitro* sustained release of AICAR and the degradation rate

To confirm the integration of AICAR in the vascular grafts, an FTIR examination was carried out. Distinct characteristic peaks, located at 1644 cm^{-1}, 1544 cm^{-1}, and 1024 cm^{-1}, were generated by vibration of the molecular bonds in AICAR, and are shown in Fig. 2A. In accordance with a previous study, wavelengths of 1629 cm^{-1} and 1556 cm^{-1} were generated by vibration of C═C and C═N bonds, respectively,[34] in AICAR, indicating that our fabricated vascular grafts contained AICAR.

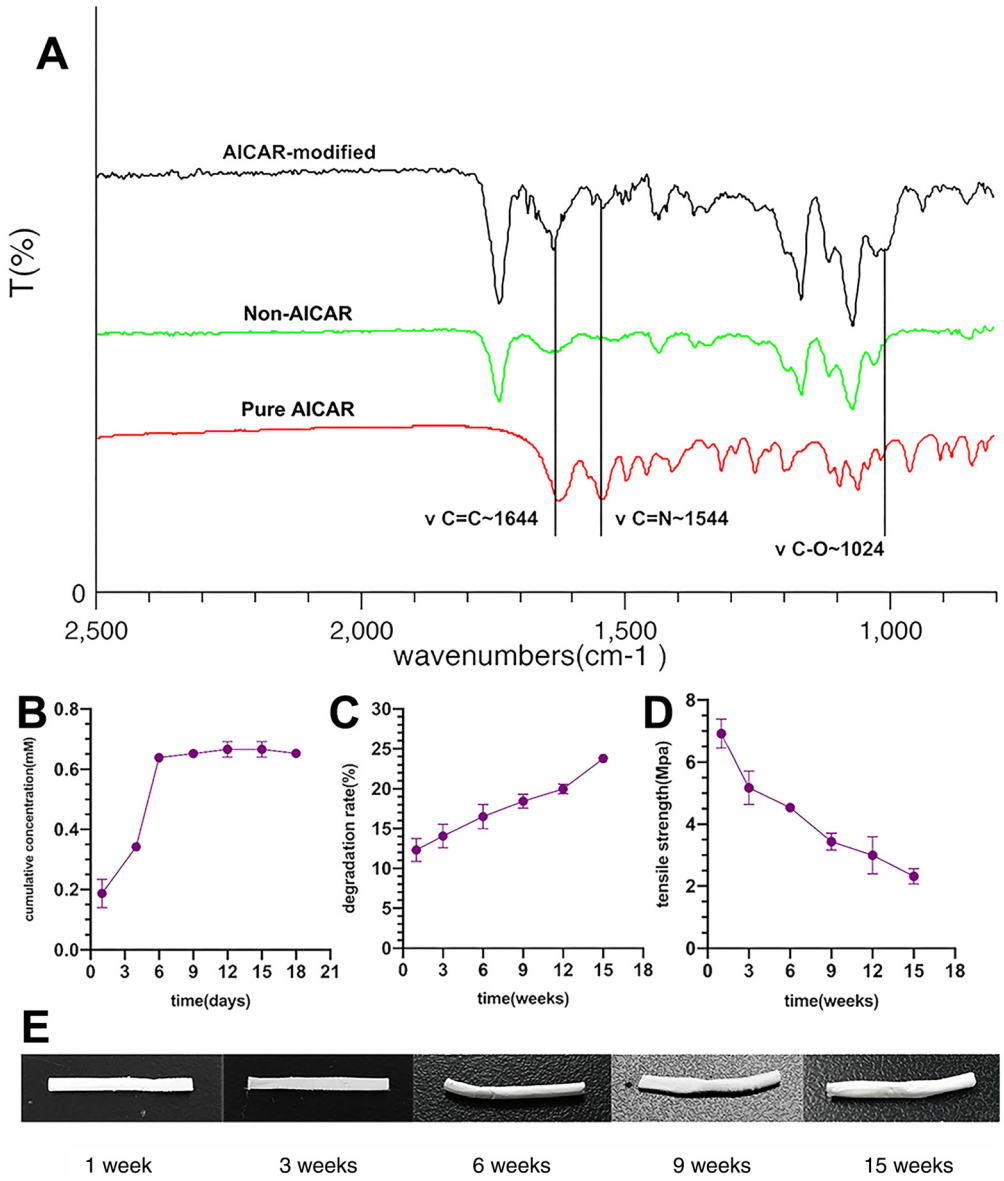

Fig. 2 Chemical and physical characterization of the fabricated vascular grafts. (A) The AICAR-modified grafts were analyzed by Fourier transform infrared spectroscopy (FTIR). The distinct characteristic peaks caused by the molecular bonds in the AICAR and AICAR-modified grafts, and their wave numbers are marked. (B) Release test of the AICAR-modified vascular grafts *in vitro* (n = 3). (C and D) The degradation rate of the vascular grafts (n = 4) and their corresponding residual tensile strength (n = 3) at each time point. (E) The visualized vascular grafts at the corresponding time point in the degradation analysis.

Release experiments indicated that approximately 50% of AICAR was released within the first 4 days. The AICAR-modified vascular grafts could sustainably release AICAR for nearly 9 days. F. Zhang *et al.* pointed out that the acute inflammatory phase occurs on days 1 to 7 after vascular transplantation.[35] The pattern of AICAR release supported that the released AICAR could act pharmacologically *in situ* in the acute inflammatory phase (Fig. 2B).

The electrospun graft degradation rate is presented in Fig. 2C. Results showed that the percentage of mass loss was fairly rapid and reached approximately 12% in the first week, mainly because of the rapid degradation of the blended gelatin. Thereafter, the degradation rate slowed to about 1.5% every 2 weeks. At the end of 15 weeks, mass loss increased by 24%. Moreover, the residual tensile strength of each sample at the corresponding time point was measured (Fig. 2D) and each sample was photographed (Fig. 2E). After 15 weeks, the tensile strength still reached approximately 3 MPa, which was close to the mechanical properties of human native small-diameter blood vessels.

3.5 AICAR achieved a better energy supply and anti-inflammatory performance of HUVECs *in vitro*

Previous studies have indicated that attenuation of endothelial cell injury can be regulated by AMPK phosphorylation.[36,37] However the potential mechanisms were not completely clear. In our study, western blotting was performed to evaluate the level of AMPK phosphorylation in each group. It was not surprising that the expression of p-AMPK was remarkably increased in the AICAR group when compared with the control and inhibitor groups (Fig. 3A). It has been reported that AMPK activation results in cellular energy increase in various cell and animal models.[38–41] Therefore, we detected the effects of AICAR on the energy supply of HUVECs. In LPS-treated HUVECs, intracellular ATP concentrations were measured. The concentration of ATP in the AICAR group was significantly higher than that of the inhibitor and control groups, whereas there were no significant differences between the control and inhibitor groups (Fig. 3B). In addition, mitochondrial membrane potential (MMP) was assessed using a JC-1 probe. The MMP was repressed in HUVECs after incubation with LPS and was significantly increased after AICAR treatment, which was similar to the change of ATP detection (Fig. 3C). These results indicated that the energy supply of HUVECs could be enhanced by AICAR, an effect that was blocked by the inhibition of AMPK using compound C. Compound C was usually utilized to prevent the effects of AICAR in AMPK phosphorylation in different cell models which were consistent with our findings.[42–44] To further investigate whether the upregulation of energy supply contributed to promoting the resolution of inflammation, the effects of AICAR on the production of the pro-inflammatory mediators, IL-6 and IL-8, in HUVECs were evaluated using ELISA kits and qRT-PCR. The protein and mRNA expressions of IL-6 and IL-8 in the AICAR group were significantly lower than those of the control and inhibitor groups (Fig. 3D). ATP synthesis is precisely regulated by the functions of the mitochondria respiratory chain complex I, II, III, and IV, and is directly associated with cell activity. Mu *et al.* found that dexmedetomidine, *via* the activation of AMPK, inhibited chronic constriction injury- (CCI-) induced decrease of the mitochondria respiratory chain complexes I, II, III, and IV, and the repression of ATP in the dorsal horn of the spinal cord.[45] AMPK is a key regulator of energy production in most cells. Koyani *et al.* also claimed that the enhanced energy supply and anti-inflammatory action improved cardiovascular function *via* AMPK activation induced by empagliflozin *in vivo* and *in vitro*.[38] Previous studies have well illustrated that AICAR is an AMPK agonist.[44,46] Moreover, Ye *et al.* revealed that NAD (H)-loaded nanoparticles improved cellular energy supply, suppressed inflammation, and prevented inflammation-induced cell apoptosis and pyroptosis.[47] ATP, viewed as a "molecular unit of currency" for intracellular energy transfer, is a dominant energy source that participates in most biological processes. These prior efforts all indicated that elevated cellular energy supply was good for cell bio-function under inflammatory conditions, even though the detailed molecular mechanism is not clearly demonstrated. Altogether, these results suggested that AICAR was thus able to protect HUVECs from inflammation, which was most likely associated with the energy supply increase.

3.6 AICAR induced MΦ polarization toward an anti-inflammatory M2 phenotype *in vitro*

Previous research studies have confirmed that MΦ reprogramming from classically activated M1 MΦ (labeled with iNOS) to alternatively M2 MΦ (labeled with CD163) contributes to tissue remodeling.[22,23] Under LPS-induced inflammation conditions, we investigated the effects of AICAR on MΦ polarization using immunofluorescence staining of iNOS and CD163 (Fig. 4A). MΦ polarization was regulated by the addition of AICAR, with a transformation rate of iNOS-M1 change from 60.1% to 17.2% and CD163-M2 change from 22.9% to 70.7%. The AICAR inhibitor reversed these effects (Fig. 4B). Moreover, the results of iNOS and CD163 mRNA expressions also confirmed this finding (Fig. 4C).

3.7 The capacity of AICAR to enhance HUVEC viability, migration and angiogenesis

EC migration and survival are important initiating events for rapid endothelialization in vascular graft replacement therapy.[48] To assess the effect of AICAR on EC migration ability, an *in vitro* wound scratch test was carried out. The images of the scratch before and after the test are shown in Fig. 5A, and the analysis is shown in Fig. 5B. The AICAR group showed the greatest migration ability among all the groups, while the inhibitor group showed the least. A similar result was also found in the transwell assay, which demonstrated that AICAR-modified vascular grafts could induce EC migration depending on the release of AICAR (Fig. S3A and B, ESI†). The effects of AICAR on HUVEC viability were determined by CCK-8 assays. In LPS-treated HUVECs, the optical density (OD) value of the AICAR group was significantly higher

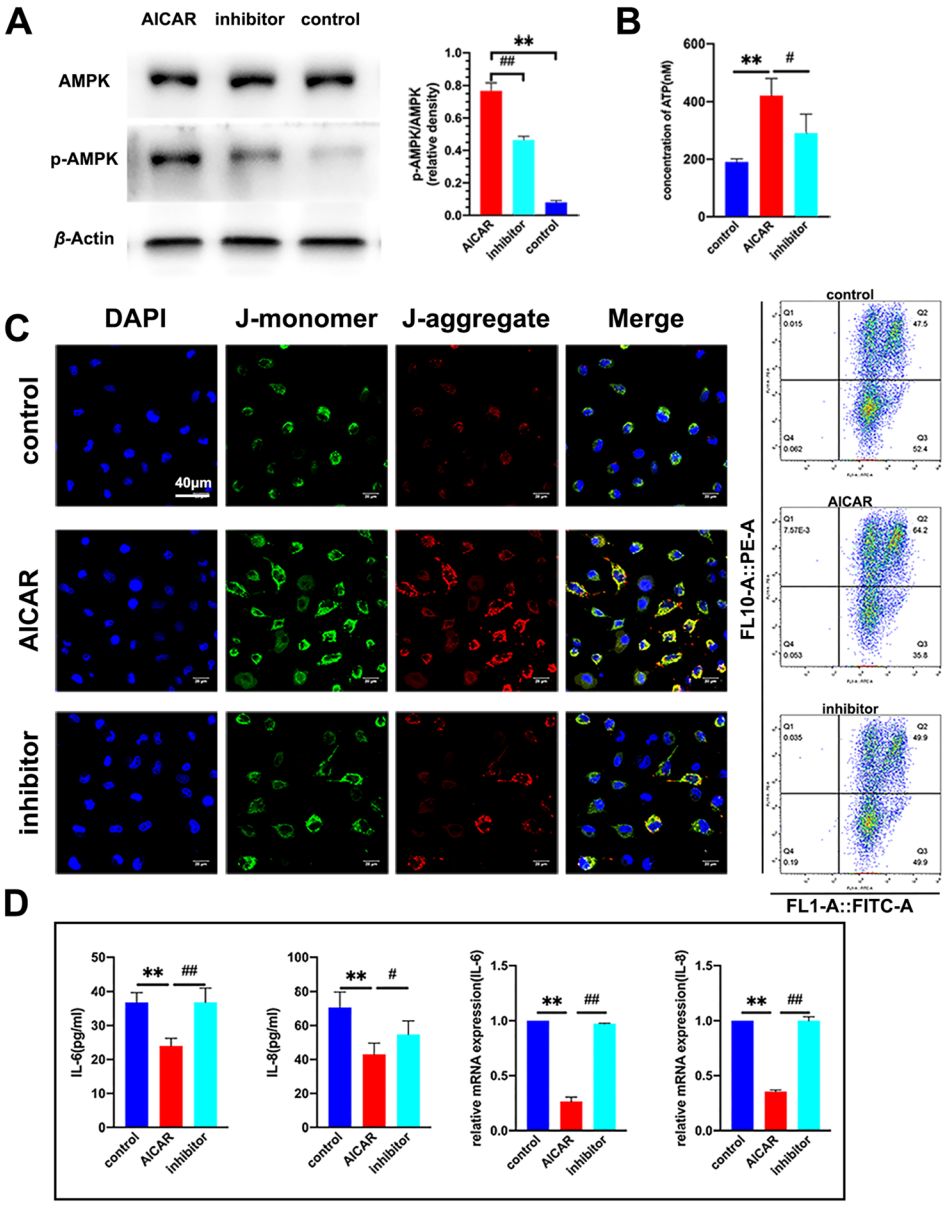

Fig. 3 AICAR strengthened the energy supply and exhibited anti-inflammatory ability on HUVECs *in vitro*. (A) The level of AMPK phosphorylation was evaluated in each group. (B) The intracellular ATP concentration of HUVECs was measured. (C) Mitochondrial Membrane Potential (MMP) was detected by laser confocal scanning microscopy and flow cytometry. (D) Quantification of IL-6/IL-8 secretion and mRNA expression. $^{**}p < 0.01$, $^{\#\#}p < 0.01$ and $^{\#}p < 0.05$ *versus* the AICAR group. The results are expressed as mean ± SD, $n \geq 3$.

than those of the inhibitor and control groups. The OD value of the inhibitor group was lower compared with that of the control group (Fig. 5D). What's more, we observed that more HUVECs adhered on the AICAR-modified membrane and evidently decreased in the control and inhibitor groups (Fig. 5C), of which the results were consistent with the CCK-8 assay. These results suggested that the addition of AICAR could protect HUVECs from inflammatory conditions, an effect that was blocked by the inhibition of AMPK by compound C.

To further detect the influence of AICAR on angiogenesis, a HUVEC tube formation assay was performed. As we expected, under the inflammatory conditions, the tube-formation capacity of HUVECs in the AICAR group was better than that of the other groups (Fig. 5F and G). Our results demonstrated that AICAR was able to ameliorate HUVEC viability, migration, and angiogenesis. Combined with the findings above, the underlying mechanism of AICAR may be associated with good energy supply and anti-inflammatory performance.

3.8 AICAR improved the *in vivo* patency rate of electrospun vascular grafts

To verify the effects of AICAR on the patency of implanted grafts, vascular grafts were sutured into the right CCA of rabbits (Fig. S4A and B and Video S1, ESI†). At 6 and 12 weeks,

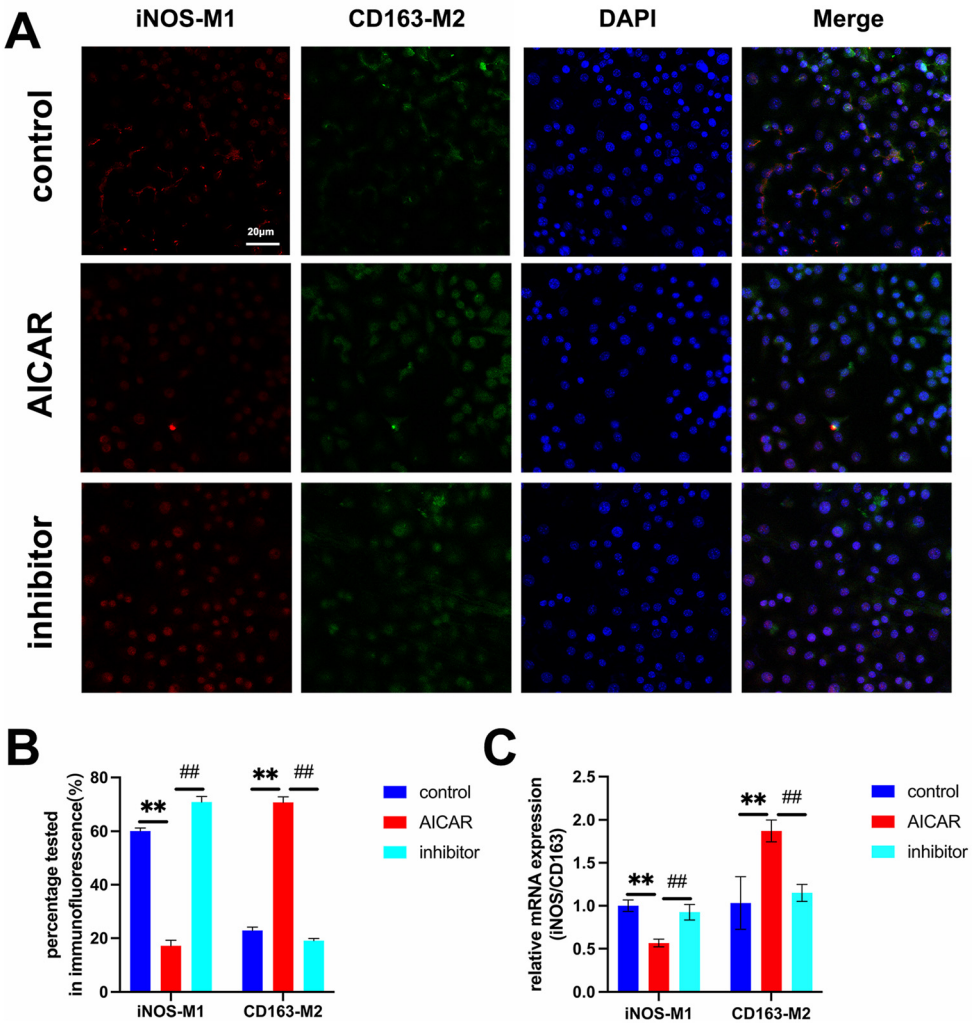

Fig. 4 AICAR reprogrammed macrophages (MΦ) to assume an anti-inflammatory phenotype. (A and B) Immunofluorescence staining of iNOS and CD163 in MΦ and quantitative analysis of the transformation rate of MΦ (n = 5). (C) Quantification of iNOS/CD163 mRNA expression (n = 3). $^{**}p$ < 0.01 and $^{\#\#}p$ < 0.01 *versus* the AICAR group. The results are expressed as mean ± SD.

the patency rate was determined using color Doppler ultrasound (Fig. 6A). Data are presented in Table S3 (ESI†). The results demonstrated that the patency rates of the AICAR groups (92.9% (13 of 14) at 6 weeks and 85.7% (6 of 7) at 12 weeks) were significantly higher than those of the control groups (11.1% (1 of 9) at 6 weeks and 0 (0 of 4) at 12 weeks). To detect whether the blood flow was similar between the right (implanted graft site) and left common carotid artery in the same rabbit model, we measured the blood flow velocity at different time points in the AICAR group. As shown in Fig. 6B, the mean blood flow velocity of the left (41.4 cm s^{-1}) and right (38.8 cm s^{-1}) common carotid arteries at 6 weeks showed no significant difference, while at 12 weeks, that of the right site (26.0 cm s^{-1}) was a little lower compared to that of the left side (35.4 cm s^{-1}). Moreover, DSA results were obtained at 12 weeks and are shown in Fig. 6C, which confirmed patency in the AICAR group and obstruction in the control group. These results suggested that the addition of AICAR in the synthetic grafts significantly increased the patency rate of the grafts, even though the blood flow velocity in the AICAR-modified grafts became a little lower in the long term.

3.9 AICAR induced better intimal tissue regeneration and endothelialization *in vivo*

To explore why AICAR achieved a better patency rate *in vivo*, the histological changes of the implanted grafts were evaluated. The grafts were explanted at 6 and 12 weeks and utilized for H&E and Masson's trichrome staining. As can be seen from Fig. 7A, the dissection of grafts showed that the AICAR-modified grafts maintained a normal morphology and blood patency compared to the untreated grafts. More evidence is shown in Fig. 7B. At 6 and 12 weeks, the AICAR groups retained patency and no visual thrombus was found in the lumen of the grafts. Moreover, the quantitative analysis of neointimal thickness in the AICAR group and control group is shown in Fig. 7C. AICAR-modified grafts had better intimal

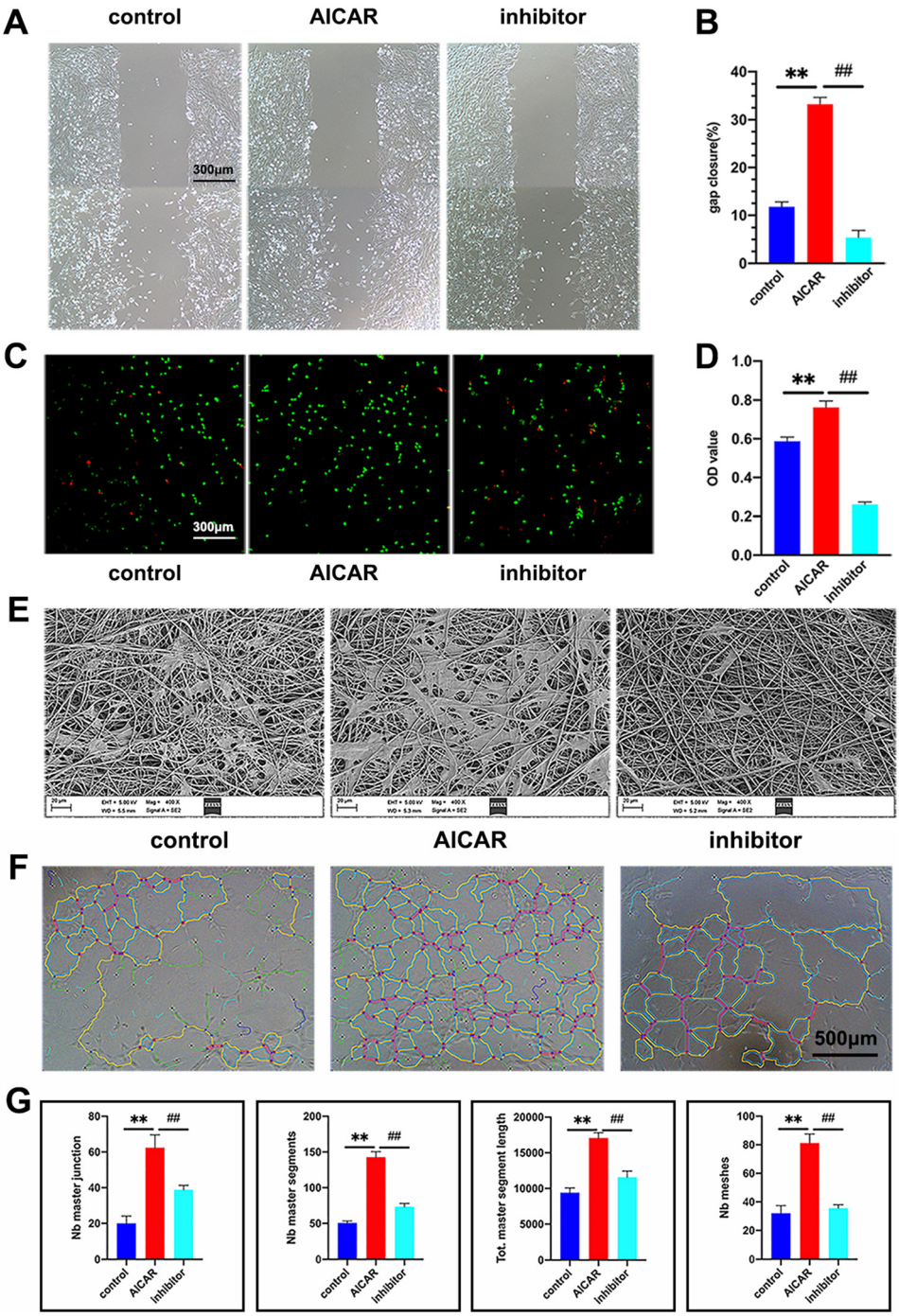

Fig. 5 *In vitro* study of AICAR's effects on HUVECs under inflammatory conditions. (A) A scratch test was performed to assess the migration ability of HUVECs in the different groups. (B) The quantitative analysis of gap closure (n = 3). (C and D) The viability of HUVECs cultured on the AICAR-modified membrane and quantitative measurement of the CCK-8 assay (n = 4). (E) The adhesion of HUVECs on the AICAR-modified membrane. (F and G) Representative pictures and quantitative estimation of the tube formation assay (n = 5). $^{**}p < 0.01$, $^{\#\#}p < 0.01$ and $^{\#}p < 0.05$ *versus* the AICAR group. The results are expressed as mean ± SD.

tissue regeneration than untreated grafts. A layer of matrix deposition was formed on the inner surface of TEVGs, which offered a favorable microenvironment for subsequent EC attachment. It is worth mentioning that some visual stratification appeared at 6 and 12 weeks, which might have resulted in the loss of mechanics and would eventually result in the collapse of lumen or graft wall expansion. The grafts showed poorer patency in the control groups compared with the AICAR groups at both 6 and 12 weeks. Obvious thrombus-like tissue formed and resulted in poor or nonexistent blood flow signals,

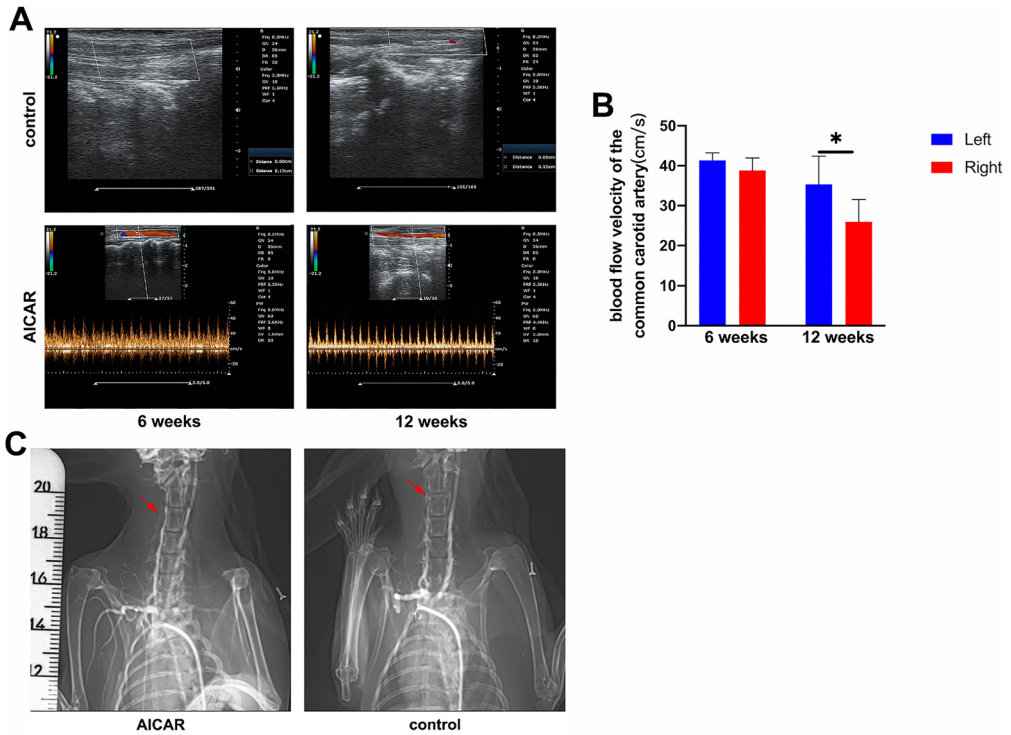

Fig. 6 Patency rate of the fabricated vascular grafts was assessed by color Doppler ultrasound and digital subtraction angiography (DSA). (A) Compared to the control group, the vascular grafts of the AICAR group were unobstructed at 6 and 12 weeks after transplantation. (B) Statistical analysis of the blood flow velocity of the left and right (implanted graft site) common carotid arteries in the AICAR group (n = 5). *p < 0.05. The results are expressed as mean ± SD. (C) The implanted grafts were confirmed to be unobstructed or obstructed by DSA 12 weeks after transplantation *in vivo*. The red arrows point at the implanted graft site.

determined by using ultrasound and DSA. In addition, the lumen of the grafts collapsed at 12 weeks and it was likely due to the lack of radial strength which resulted from inadequate ECs and ECM attachment to the inner surface. In the vascular graft walls, more severe inflammatory cell infiltration was found in the control groups than in the AICAR groups (Fig. 7D). The lymphocyte, macrophage and neutrophil cells were counted and the results indicated that AICAR could promote inflammation resolution, which contributed to EC survival and quick endothelialization.

To further confirm that AICAR contributed to vascular remodeling, at 12 weeks, immunofluorescence staining of CD31 and α-SMA was performed to visualize ECs and VSMCs within the implanted TEVGs. Compared to untreated grafts, more visual capillary formation was seen on the abluminal surface of the AICAR-modified grafts. Yellow arrows point to the capillaries (Fig. 8A). Statistical analysis showed that the number of capillaries of the AICAR-modified grafts was 8.80 ± 1.79 per high-powered field (hpf), which was approximately 2-fold that of the untreated grafts (Fig. 8B). The EC numbers on the luminal surface of the AICAR-modified grafts were also significantly higher than those of the untreated grafts (Fig. 8C). These findings indicated that the addition of AICAR could significantly promote EC adhesion and capillary formation. These outcomes were considered to be crucial for vascular regeneration.[21,49,50] Representative CD31 and α-SMA staining images of the cross-section and longitudinal section of the AICAR-modified grafts are shown in Fig. 8D. Endothelialization of the AICAR group and control group was observed by SEM at 12 weeks (Fig. 8E). The statistical analysis of EC coverage is shown in Fig. 8F. As expected, the data confirmed a higher coverage rate of ECs on the AICAR-modified grafts (~89.9%) compared with the control grafts (~62.8%). These findings demonstrated that AICAR promoted endothelialization *in vivo*. We believed that the EC monolayer was helpful for inhibiting thrombosis and increasing patency.

3.10 AICAR reprogrammed MΦ into an anti-inflammatory M2 phenotype in the vascular wall

The process of tissue regeneration after transplantation is associated with MΦ polarization. It is established that M2 MΦ possesses the ability to facilitate tissue repair and regeneration.[51] We performed immunofluorescence staining of iNOS and CD163 to evaluate MΦ infiltration in the grafts at 6 and 12 weeks (Fig. 9A). We found that the percentage of CD163-M2 was higher than that of iNOS-M1 in all grafts at 6 and 12 weeks. The ratio of CD163 : iNOS MΦ, presented in the AICAR-modified vascular graft wall was significantly higher than that of the control group (Fig. 9B). These results demonstrated that

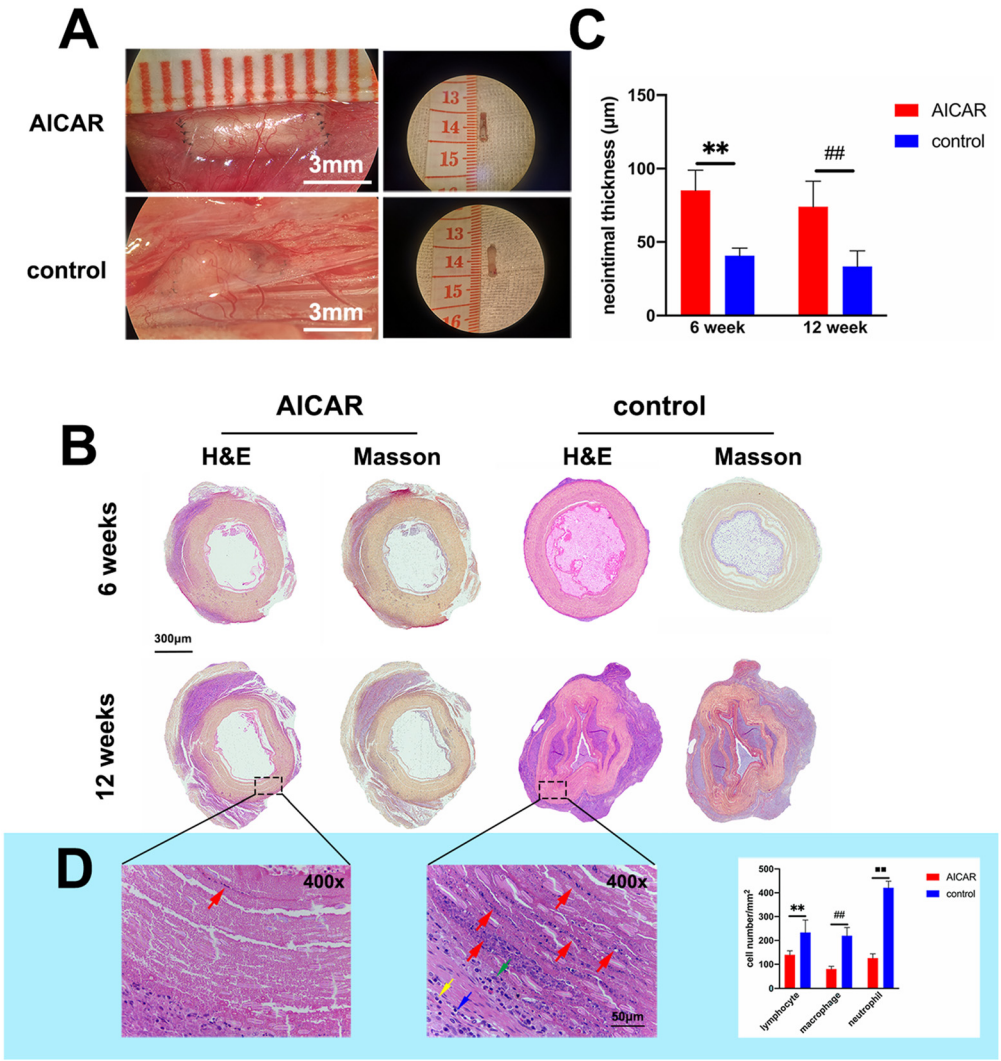

Fig. 7 Histological changes of the implanted grafts at 6 or 12 weeks. (A) Dissection of the implanted grafts at 12 weeks. (B) Representative H&E and Masson's trichrome staining images of the cross-sections of the explanted grafts. AICAR-modified vascular grafts remained open and a layer of matrix deposition was present within the inner surface at 6 and 12 weeks, while the untreated vascular grafts were blocked and obvious thrombus-like tissue was found within the lumen. Masson: collagen = blue, graft = yellow. (C) Quantitative analysis of neointimal thickness at 6 and 12 weeks in the different groups (n = 5). **p < 0.01 and $^{\#\#}p$ < 0.01. The results are expressed as mean ± SD. (D) H&E staining of the cross-sections of the explanted grafts at 12 weeks and the quantitative comparison of lymphocyte, macrophage, and neutrophil cells in the different groups. n = 5, **p < 0.01, $^{\#\#}p$ < 0.01 and ■■p < 0.01. The results are expressed as mean ± SD. The red arrows indicate severe inflammatory cell infiltration in the walls of vascular grafts (blue arrow: lymphocytes; green arrow: macrophages; yellow arrow: neutrophils).

AICAR-modified vascular grafts induced more anti-inflammatory M2 MΦ similar to the *in vitro* performance.

4. Discussion

Rapid endothelialization has been a great challenge in small-diameter vascular graft fabrication and is yet to be fully resolved.[8,52] Previous studies have indicated that promoting inflammation resolution contributes to endothelial cell survival and sufficient subsequent endothelialization.[19,20] To date, there have been no studies on associating cellular energy supply with anti-inflammation reaction in the field of vascular regeneration. In our study, an AMPK activator (AICAR) with the ability to maintain energy supply and induce MΦ into an anti-inflammatory phenotype was utilized to functionalize the fabricated vascular grafts. A rabbit CCA replacement model was used to evaluate the *in vivo* performance of the grafts and we demonstrated that the AICAR-modified small-diameter TEVGs improved the patency rate at 6 and 12 weeks compared with the untreated grafts. Moreover, *in vivo* implanted grafts of the AICAR groups showed better endothelialization and vascular regeneration.

In the past several decades, great efforts have been devoted to developing TEVGs in the manufacturing methods and surface modifications. However, vascular implantation and

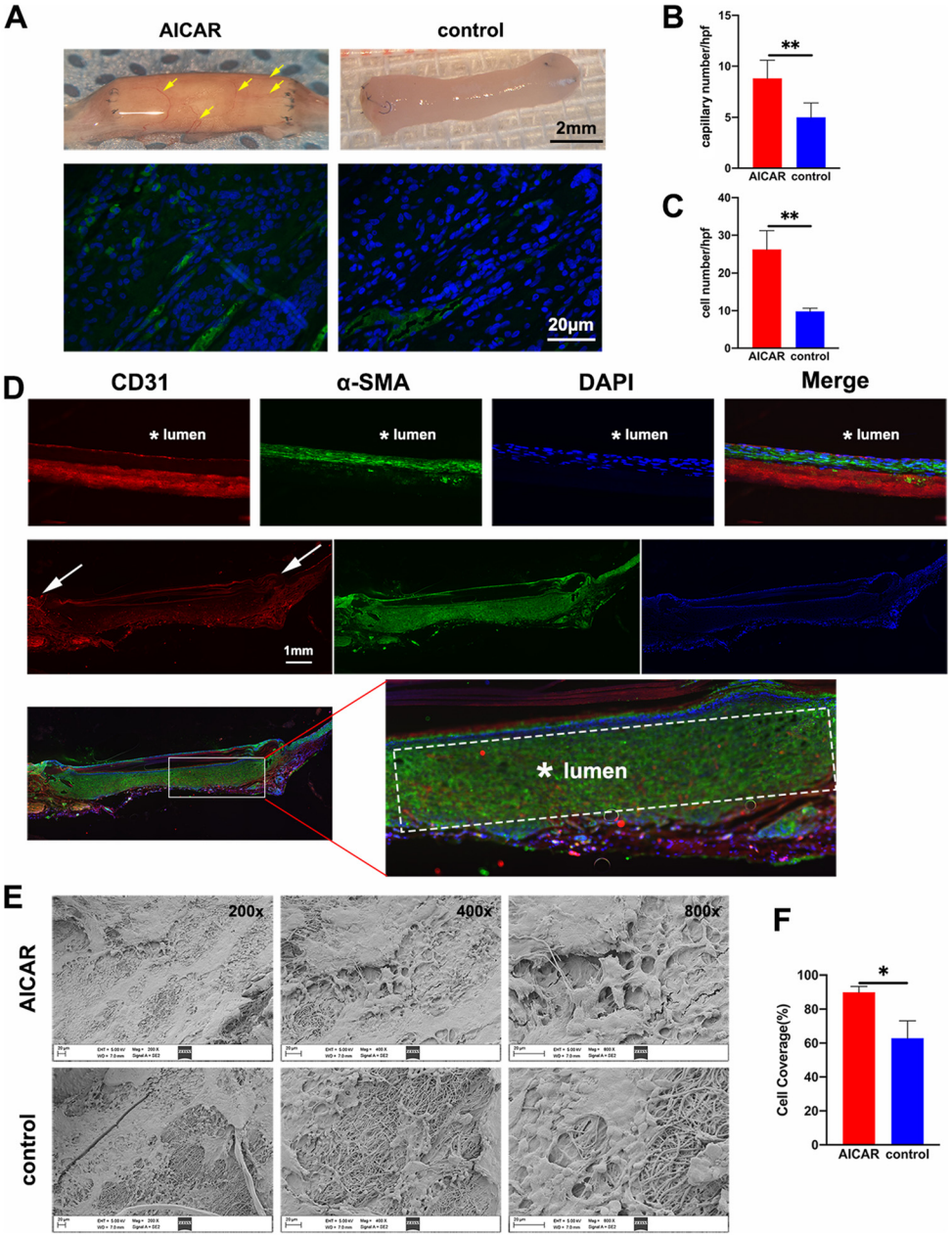

Fig. 8 Evaluation of vascular remodeling in the grafts at 12 weeks post-implantation. (A) Visual capillary formation on the abluminal surface of the explanted grafts. The yellow arrows point to the capillaries. And immunofluorescence staining of CD31 (green) co-localized with DAPI (blue) on the intima in the grafts in each group. (B and C) Quantitative comparison of the capillary number (B) and cell number (C) between the AICAR group and the control group (n = 5). (D) Representative CD31 staining (red) and α-SMA staining (green) images of the cross-section and longitudinal section of the explanted grafts in the AICAR group. Nuclei are stained with DAPI (blue). White arrow: the anastomosis site; *: lumen; (E) SEM micrographs of ECs spread on the inner lumen. (F) The analysis data of EC coverage in the different groups (n = 3). *p < 0.05 and **p < 0.01. The results are expressed as mean ± SD.

immune rejection of vascular grafts inevitably damage ECs in blood vessels and invoke an inflammatory response, thereby causing endothelial energy depletion and insufficient endothelialization.[53] AMPK is a central regulator of multiple metabolic pathways and has been shown to have therapeutic importance in the treatment of several diseases associated with chronic and acute inflammation.[38,39] An AMPK activator (AICAR) has been reported to have anti-inflammatory effects on several cell types and, importantly, AMPK activators have been found to ameliorate inflammation-induced endothelial dysfunction.[28,29,54] Hence, we hypothesized that the addition of AICAR in the fabricated vascular grafts might protect ECs. In the present study, AICAR-modified vascular grafts were successfully fabricated by the co-electrospinning technique. The

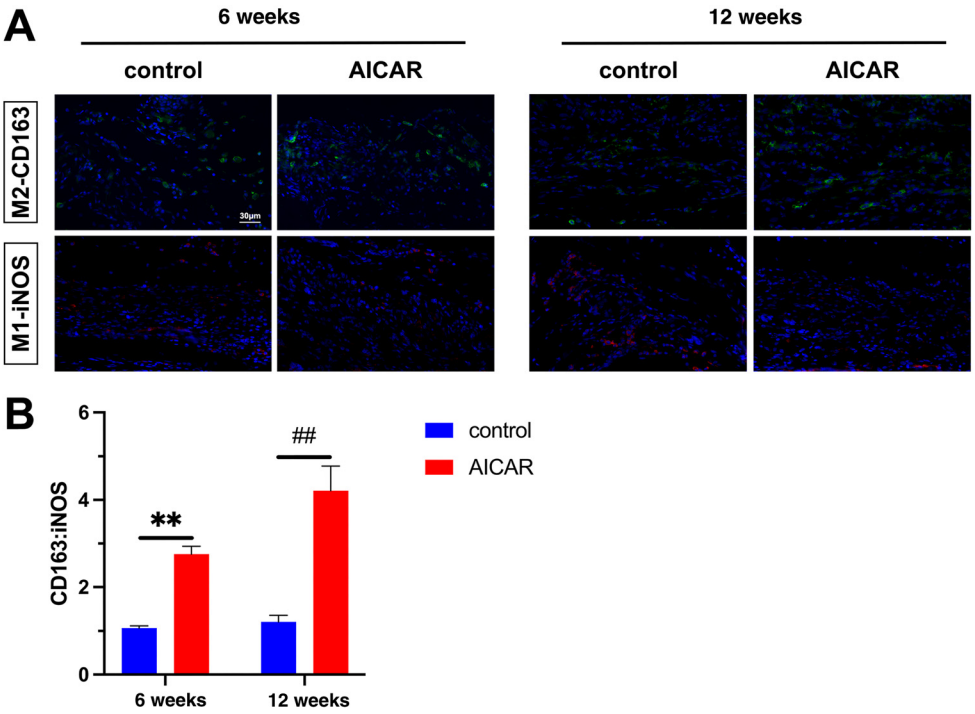

Fig. 9 The infiltration of MΦ phenotypes in the vascular wall during the process of vascular remodeling. (A) Immunofluorescence staining of iNOS-M1 (red) and CD163-M2 (green) in the grafts at 6 and 12 weeks. Nuclei are stained with DAPI (blue). (B) Quantification of the ratio of the percentage of CD163 : iNOS macrophages infiltrated in the remodeled grafts at various time points after implantation (n = 3). $^{**}p < 0.01$ and $^{\#\#}p < 0.01$. The results are expressed as mean ± SD.

release of AICAR from the grafts lasted at least for 9 days, which demonstrated that AICAR was able to exhibit pharmacological effects *in situ* in the acute inflammatory phase. In LPS-induced HUVECs, the bioactivity of AICAR was assessed. We found that AICAR significantly improved the cellular energy status by inducing AMPK phosphorylation under inflammatory conditions. The secretion of pro-inflammatory cytokines (IL-6 and IL-8) was down-regulated after AICAR treatment. These data suggested that AICAR upregulated endothelial cellular ATP and attenuated the inflammatory reaction, which could contribute to the survival of regenerative cells during vascular graft remodeling. In addition, we found that treatment with AICAR supported the survival of HUVECs and adhesion on the electrospun membrane under inflammatory conditions. What's more, AICAR improved the capacity of migration and angiogenesis *in vitro* according to the scratch test and tube formation assay. Overall, AICAR exhibited a promising pharmacological therapeutic effect to ensure better regenerative potential *in vitro*.

Importantly, *in vivo* implantation also showed better remodeling processes in the AICAR-modified vascular grafts. It has been previously reported that quick endothelialization plays an essential role in vascular graft survival, as the endothelial cell layer can inhibit thrombosis and inflammation.[49,50,55] At 12 weeks post-implantation, more endothelial cells grew on the AICAR-modified grafts. Interestingly, there was more matrix deposition but without obvious thrombus-like tissues in the AICAR group. These good outcomes could be attributed to the rapid endothelialization, avoiding possible subsequent thrombosis in the AICAR-modified grafts. Sufficient vascularization within the implanted tissue-engineered constructs contributes to favorable tissue regeneration.[56] After 12-week implantation, immunofluorescence staining of CD31 and visual capillary formation on the abluminal surface of explanted grafts indicated that more neocapillaries were formed in the AICAR group. The immunofluorescence staining of α-SMA indicated that some contractile VSMCs grew within the graft wall. Moreover, the data of color Doppler ultrasound and digital DSA confirmed the better outcome of AICAR-modified grafts, as AICAR significantly improved the patency rate of grafts at 6 or 12 weeks post-implantation. These results confirmed that the addition of AICAR achieved a promising vascular remodeling and higher patency rate.

In addition to our finding that AICAR strengthened the cellular energy supply, which resulted in favorable regenerative potential, promoting inflammation resolution is regarded as an efficient way to encourage tissue remodeling. Despite some evidence suggesting that acute inflammation initiates the regenerative process,[57] accumulating studies have revealed that excessive or prolonged inflammation can negatively contribute to vascular remodeling.[19,20] Promoting inflammation resolution by macrophages (MΦ) is necessary for the survival of regenerative cells. Recent studies have confirmed that an M2 anti-inflammatory phenotype can be induced by AMPK phosphorylation in the study of myocardial infarction, neuroinflammation and lung carcinoma.[58–60] However, whether AMPK

phosphorylation induced MΦ into an M2 anti-inflammatory phenotype in the field of vascular replacement therapy was not well established. In this study, LPS stimulated MΦ into an M1 pro-inflammatory phenotype *in vitro*, whereas this effect was reversed by the treatment of AICAR. Moreover, we observed the anti-inflammatory performance of the AICAR-modified grafts *in vivo*. At 12 weeks, there was more severe inflammatory cell infiltration in the control group. In contrast, milder inflammation was found within the AICAR-modified grafts. Importantly, we observed a similar change for the infiltration of MΦ in the implanted grafts, as MΦ polarization of the AICAR group manifested a distinct anti-inflammatory phenotype (CD163-M2); inversely, more pro-inflammatory phenotypes (iNOS-M1) MΦ were found within the control group. MΦ polarization toward an anti-inflammatory phenotype attenuates inflammation and favors tissue remodeling,[61] which was also observed in our study.

In summary, our findings revealed a novel approach to functionalize vascular grafts, which gave the capacity to elevate cellular energy and promote inflammation resolution by MΦ polarization. The AICAR-modified vascular grafts obtained quick endothelialization and favorable vascular remodeling potential. This effect was likely attributed to AMPK phosphorylation. Additionally, it is worth noting that we did not investigate how the possible downstream effector proteins function following AMPK phosphorylation. This needs to be determined in further studies.

5. Conclusions

In our work, ECs treated with AICAR were able to achieve sufficient energy supply and had better migration, viability, and angiogenesis in the inflammatory microenvironment compared with the controls. Additionally, AICAR-modified small-diameter TEVGs were successfully generated by electrospinning, and the addition of AICAR contributed to a higher patency rate at 6 and 12 weeks, which was related to increased endothelialization and inflammation resolution by MΦ polarization. In clinical vascular replacement, a severe inflammation state often results in thrombosis and blockage of grafts. Overall, this study opens a new possibility for promoting the regeneration of small-diameter vascular grafts *via* promoting energy supply and anti-inflammatory mechanisms.

Author contributions

Hengxian Su, Wenchao Liu, and Xifeng Li: investigation, conceptualization, data curation, writing – original draft, and project administration; Guangxu Li, Shenquan Guo, Chang Liu, and Chubin Ou: data curation and visualization; Tao Yang, Jiahui Liu, Yuanzhi Li, and Chengcong Wei: data curation and resources; and Chuanzhi Duan, Tao Xu, and Qing Huang: conceptualization, methodology, supervision, project administration, and funding acquisition.

Conflicts of interest

All authors declare no competing financial interest.

Acknowledgements

This work was supported by the National Key Research Development Program (grants 2016YFC1300804 and 2016YFC1300800), the Science and Technology Project Foundation of Guangdong Province (grant 2016A020215098), the National Natural Science Foundation of China (no. 81974178 and 82001300), the National Natural Science Foundation Special Research of Tongzhou Science and Technology Project (KJ2019CX014-02), the Tongzhou Yunhe Project in Health Field of Beijing (2017B0400104) and the Introduced and Jointly Built High-end R&D Institute of Jiangxi (grant 20203CCH45008).

References

1 G. B. Perera, M. P. Mueller, S. M. Kubaska, S. E. Wilson, P. F. Lawrence and R. M. Fujitani, Superiority of autogenous arteriovenous hemodialysis access: maintenance of function with fewer secondary interventions, *Ann. Vasc. Surg.*, 2004, **18**, 66–73.
2 J. Fajadet and A. Chieffo, Current management of left main coronary artery disease, *Eur. Heart J.*, 2012, **33**, 36b–50b.
3 N. R. Holm, T. Mäkikallio, M. M. Lindsay, *et al.*, Percutaneous coronary angioplasty versus coronary artery bypass grafting in the treatment of unprotected left main stenosis: updated 5-year outcomes from the randomised, non-inferiority NOBLE trial, *Lancet*, 2020, **395**, 191–199.
4 A. Hasan, A. Memic, N. Annabi, *et al.*, Electrospun scaffolds for tissue engineering of vascular grafts, *Acta Biomater.*, 2014, **10**, 11–25.
5 S. Pashneh-Tala, S. MacNeil and F. Claeyssens, The Tissue-Engineered Vascular Graft-Past, Present, and Future, *Tissue Eng., Part B*, 2016, **22**, 68–100.
6 M. S. Conte, Critical appraisal of surgical revascularization for critical limb ischemia, *J. Vasc. Surg.*, 2013, **57**, 8s–13s.
7 V. S. Chernonosova, P. P. Laktionov, I. S. Murashov, A. A. Karpenko and P. P. Laktionov, Comparative gene expression profiling of human primary endotheliocytes cultivated on polyurethane-based electrospun 3D matrices and natural decellularized vein, *Biomed. Mater.*, 2020, **15**, 045012.
8 D. Wang, Y. Xu, Q. Li and L. S. Turng, Artificial small-diameter blood vessels: materials, fabrication, surface modification, mechanical properties, and bioactive functionalities, *J. Mater. Chem. B*, 2020, **8**, 1801–1822.
9 B. Yi, Y. Shen, H. Tang, X. Wang and Y. Zhang, Stiffness of the aligned fibers affects structural and functional integrity of the oriented endothelial cells, *Acta Biomater.*, 2020, **108**, 237–249.

10 Y. Zhuang, C. Zhang, M. Cheng, *et al.*, Challenges and strategies for in situ endothelialization and long-term lumen patency of vascular grafts, *Bioact. Mater.*, 2021, **6**, 1791–1809.
11 D. Radke, W. Jia, D. Sharma, *et al.*, Tissue Engineering at the Blood-Contacting Surface: A Review of Challenges and Strategies in Vascular Graft Development, *Adv. Healthc. Mater.*, 2018, **7**, e1701461.
12 H. Yuan, C. Chen, Y. Liu, T. Lu and Z. Wu, Strategies in cell-free tissue-engineered vascular grafts, *J. Biomed. Mater. Res., Part A*, 2020, **108**, 426–445.
13 S. Jana, Endothelialization of cardiovascular devices, *Acta Biomater.*, 2019, **99**, 53–71.
14 K. S. Washington and C. A. Bashur, Delivery of Antioxidant and Anti-inflammatory Agents for Tissue Engineered Vascular Grafts, *Front. Pharmacol.*, 2017, **8**, 659.
15 D. Tang, S. Chen, D. Hou, *et al.*, Regulation of macrophage polarization and promotion of endothelialization by NO generating and PEG-YIGSR modified vascular graft, *Mater. Sci. Eng., C*, 2018, **84**, 1–11.
16 Y. Wei, Y. Wu, R. Zhao, *et al.*, MSC-derived sEVs enhance patency and inhibit calcification of synthetic vascular grafts by immunomodulation in a rat model of hyperlipidemia, *Biomaterials*, 2019, **204**, 13–24.
17 M. Levi, T. T. Keller, E. van Gorp and H. ten Cate, Infection and inflammation and the coagulation system, *Cardiovasc. Res.*, 2003, **60**, 26–39.
18 S. Y. Chien, C. Y. Huang, C. H. Tsai, S. W. Wang, Y. M. Lin and C. H. Tang, Interleukin-1β induces fibroblast growth factor 2 expression and subsequently promotes endothelial progenitor cell angiogenesis in chondrocytes, *Clin. Sci.*, 2016, **130**, 667–681.
19 Y. Li, S. Wan, G. Liu, *et al.*, Netrin-1 Promotes Inflammation Resolution to Achieve Endothelialization of Small-Diameter Tissue Engineering Blood Vessels by Improving Endothelial Progenitor Cells Function In Situ, *Adv. Sci.*, 2017, **4**, 1700278.
20 J. Shi, X. Zhang, L. Jiang, *et al.*, Regulation of the inflammatory response by vascular grafts modified with Aspirin-Triggered Resolvin D1 promotes blood vessel regeneration, *Acta Biomater.*, 2019, **97**, 360–373.
21 W. Liu, G. Zhang, J. Wu, *et al.*, Insights into the angiogenic effects of nanomaterials: mechanisms involved and potential applications, *J. Nanobiotechnol.*, 2020, **18**, 9.
22 T. Hasegawa, C. J. Hall, P. S. Crosier, *et al.*, Transient inflammatory response mediated by interleukin-1beta is required for proper regeneration in zebrafish fin fold, *eLife*, 2017, **6**, 1–22.
23 H. Kim, S. Y. Wang, G. Kwak, Y. Yang, I. C. Kwon and S. H. Kim, Exosome-Guided Phenotypic Switch of M1 to M2 Macrophages for Cutaneous Wound Healing, *Adv. Sci.*, 2019, **6**, 1900513.
24 A. Stahl, D. Hao, J. Barrera, *et al.*, A bioactive compliant vascular graft modulates macrophage polarization and maintains patency with robust vascular remodeling, *Bioact. Mater.*, 2023, **19**, 167–178.
25 M. Lopez, Hypothalamic AMPK as a possible target for energy balance-related diseases, *Trends Pharmacol. Sci.*, 2022, **43**, 546–556.
26 L. A. O'Neill and E. J. Pearce, Immunometabolism governs dendritic cell and macrophage function, *J. Exp. Med.*, 2016, **213**, 15–23.
27 S. M. Jeon, Regulation and function of AMPK in physiology and diseases, *Exp. Mol. Med.*, 2016, **48**, e245.
28 L. A. O'Neill and D. G. Hardie, Metabolism of inflammation limited by AMPK and pseudo-starvation, *Nature*, 2013, **493**, 346–355.
29 Y. Sun, J. Li, N. Xiao, *et al.*, Pharmacological activation of AMPK ameliorates perivascular adipose/endothelial dysfunction in a manner interdependent on AMPK and SIRT1, *Pharmacol. Res.*, 2014, **89**, 19–28.
30 D. Garcia and R. J. Shaw, AMPK: Mechanisms of Cellular Energy Sensing and Restoration of Metabolic Balance, *Mol. Cell*, 2017, **66**, 789–800.
31 C. Rodriguez, C. Contreras, J. Saenz-Medina, *et al.*, Activation of the AMP-related kinase (AMPK) induces renal vasodilatation and downregulates Nox-derived reactive oxygen species (ROS) generation, *Redox Biol.*, 2020, **34**, 101575.
32 G. Beldi, S. Bahiraii, C. Lezin, *et al.*, TNFR2 Is a Crucial Hub Controlling Mesenchymal Stem Cell Biological and Functional Properties, *Front. Cell Dev. Biol.*, 2020, **8**, 596831.
33 D. L. Donovan, S. P. Schmidt, S. P. Townshend, G. O. Njus and W. V. Sharp, Material and structural characterization of human saphenous vein, *J. Vasc. Surg.*, 1990, **12**, 531–537.
34 Y. Wu, L. Li, W. Chen, *et al.*, Maintaining Moderate Platelet Aggregation and Improving Metabolism of Endothelial Progenitor Cells Increase the Patency Rate of Tissue-Engineered Blood Vessels, *Tissue Eng., Part A*, 2015, **21**, 2001–2012.
35 F. Zhang and M. W. King, Immunomodulation Strategies for the Successful Regeneration of a Tissue-Engineered Vascular Graft, *Adv. Healthc. Mater.*, 2022, **11**, e2200045.
36 Y. L. Cui, R. Q. Xue, H. Xi, *et al.*, Cholinergic drugs ameliorate endothelial dysfunction by decreasing O-GlcNAcylation via M3 AChR-AMPK-ER stress signaling, *Life Sci.*, 2019, **222**, 1–12.
37 D. Zibrova, F. Vandermoere, O. Goransson, *et al.*, GFAT1 phosphorylation by AMPK promotes VEGF-induced angiogenesis, *Biochem. J.*, 2017, **474**, 983–1001.
38 C. N. Koyani, I. Plastira, H. Sourij, *et al.*, Empagliflozin protects heart from inflammation and energy depletion via AMPK activation, *Pharmacol. Res.*, 2020, **158**, 104870.
39 E. A. Day, R. J. Ford and G. R. Steinberg, AMPK as a Therapeutic Target for Treating Metabolic Diseases, *Trends Endocrinol. Metab.*, 2017, **28**, 545–560.
40 A. Sato, Y. Shiraishi, T. Kimura, *et al.*, Resistance to Obesity in SOD1 Deficient Mice with a High-Fat/High-Sucrose Diet, *Antioxidants*, 2022, **11**, 1403.

41 D. Wang, L. Cao, X. Zhou, *et al.*, Mitigation of honokiol on fluoride-induced mitochondrial oxidative stress, mitochondrial dysfunction, and cognitive deficits through activating AMPK/PGC-1alpha/Sirt3, *J. Hazard. Mater.*, 2022, **437**, 129381.
42 D. Hall, T. Griss, J. Ma, *et al.*, The AMPK agonist 5-aminoimidazole-4-carboxamide ribonucleotide (AICAR), but not metformin, prevents inflammation-associated cachectic muscle wasting, *EMBO Mol. Med.*, 2018, **10**, e8307.
43 J. Xiao, S. Zhu, H. Guan, *et al.*, AMPK alleviates high uric acid-induced Na-K-ATPase signaling impairment and cell injury in renal tubules, *Exp. Mol. Med.*, 2019, **51**, 1–14.
44 T. Yang, X. Wang, Y. Zhou, *et al.*, SEW2871 attenuates ANIT-induced hepatotoxicity by protecting liver barrier function via sphingosine 1-phosphate receptor-1-mediated AMPK signaling pathway, *Cell Biol. Toxicol.*, 2021, **37**, 595–609.
45 Y. Mu, Y. Mei, Y. Chen, *et al.*, Perisciatic Nerve Dexmedetomidine Alleviates Spinal Oxidative Stress and Improves Peripheral Mitochondrial Dynamic Equilibrium in a Neuropathic Pain Mouse Model in an AMPK-Dependent Manner, *Dis. Markers*, 2022, **2022**, 6889676.
46 J. Xiao, S. Zhu, H. Guan, *et al.*, AMPK alleviates high uric acid-induced Na(+)-K(+)-ATPase signaling impairment and cell injury in renal tubules, *Exp. Mol. Med.*, 2019, **51**, 1–14.
47 M. Ye, Y. Zhao, Y. Wang, *et al.*, NAD(H)-loaded nanoparticles for efficient sepsis therapy via modulating immune and vascular homeostasis, *Nat. Nanotechnol.*, 2022, **17**, 880–890.
48 D. Tousoulis, I. Andreou, C. Antoniades, C. Tentolouris and C. Stefanadis, Role of inflammation and oxidative stress in endothelial progenitor cell function and mobilization: therapeutic implications for cardiovascular diseases, *Atherosclerosis*, 2008, **201**, 236–247.
49 P. Li, D. Jin, J. Dou, *et al.*, Nitric oxide-releasing poly (epsilon-caprolactone)/S-nitrosylated keratin biocomposite scaffolds for potential small-diameter vascular grafts, *Int. J. Biol. Macromol.*, 2021, **189**, 516–527.
50 J. Zhou, M. Wang, T. Wei, *et al.*, Endothelial Cell-Mediated Gene Delivery for In Situ Accelerated Endothelialization of a Vascular Graft, *ACS Appl. Mater. Interfaces*, 2021, **13**, 16097–16105.
51 B. N. Brown, J. E. Valentin, A. M. Stewart-Akers, G. P. McCabe and S. F. Badylak, Macrophage phenotype and remodeling outcomes in response to biologic scaffolds with and without a cellular component, *Biomaterials*, 2009, **30**, 1482–1491.
52 E. C. Novosel, C. Kleinhans and P. J. Kluger, Vascularization is the key challenge in tissue engineering, *Adv. Drug Delivery Rev.*, 2011, **63**, 300–311.
53 N. Ding, C. Dou, Y. Wang, *et al.*, Antishear Stress Bionic Carbon Nanotube Mesh Coating with Intracellular Controlled Drug Delivery Constructing Small-Diameter Tissue-Engineered Vascular Grafts, *Adv. Healthc. Mater.*, 2018, **7**, e1800026.
54 I. P. Salt and D. G. Hardie, AMP-Activated Protein Kinase: An Ubiquitous Signaling Pathway With Key Roles in the Cardiovascular System, *Circ. Res.*, 2017, **120**, 1825–1841.
55 S. Yang, X. Zheng, M. Qian, *et al.*, Nitrate-Functionalized poly(epsilon-Caprolactone) Small-Diameter Vascular Grafts Enhance Vascular Regeneration via Sustained Release of Nitric Oxide, *Front. Bioeng. Biotechnol.*, 2021, **9**, 770121.
56 H. K. Wong, C. R. Ivan Lam, F. Wen, *et al.*, Novel method to improve vascularization of tissue engineered constructs with biodegradable fibers, *Biofabrication*, 2016, **8**, 015004.
57 J. D. Roh, R. Sawh-Martinez, M. P. Brennan, *et al.*, Tissue-engineered vascular grafts transform into mature blood vessels via an inflammation-mediated process of vascular remodeling, *Proc. Natl. Acad. Sci. U. S. A.*, 2010, **107**, 4669–4674.
58 S. Yan, M. Zhou, X. Zheng, *et al.*, Anti-Inflammatory Effect of Curcumin on the Mouse Model of Myocardial Infarction through Regulating Macrophage Polarization, *Mediators Inflammation*, 2021, **2021**, 9976912.
59 C. F. Tsai, G. W. Chen, Y. C. Chen, *et al.*, Regulatory Effects of Quercetin on M1/M2 Macrophage Polarization and Oxidative/Antioxidative Balance, *Nutrients*, 2022, **14**, 67.
60 S. Zhou, Y. Lan, Y. Li, Z. Li, J. Pu and L. Wei, Hypoxic Tumor-Derived Exosomes Induce M2 Macrophage Polarization via PKM2/AMPK to Promote Lung Cancer Progression, *Cell Transplant.*, 2022, **31**, 9636897221106998.
61 Y. Fu, C. Gao, Y. Liang, *et al.*, Shift of Macrophage Phenotype Due to Cartilage Oligomeric Matrix Protein Deficiency Drives Atherosclerotic Calcification, *Circ. Res.*, 2016, **119**, 261–276.